LA-UR-18-20221
Approved for public release; distribution is unlimited.

Title: Argonne Bubble Experiment Thermal Model Development III

Author(s): Buechler, Cynthia Eileen

Intended for: Report

Issued: 2018-01-11

Introduction

This report describes the continuation of the work reported in "Argonne Bubble Experiment Thermal Model Development"[1] and "Argonne Bubble Experiment Thermal Model Development II"[2]. The experiment was performed at Argonne National Laboratory (ANL) in 2014.[3] A rastered 35 MeV electron beam deposited power in a solution of uranyl sulfate, generating heat and radiolytic gas bubbles. Irradiations were performed at beam power levels between 6 and 15 kW. Solution temperatures were measured by thermocouples, and gas bubble behavior was recorded.

The previous report[2] described the Monte-Carlo N-Particle (MCNP) calculations and Computational Fluid Dynamics (CFD) analysis performed on the as-built solution vessel geometry. The CFD simulations in the current analysis were performed using Ansys Fluent, Ver. 17.2. The same power profiles determined from MCNP calculations in earlier work[2] were used for the 12 and 15 kW simulations. The primary goal of the current work is to calculate the temperature profiles for the 12 and 15 kW cases using reasonable estimates for the gas generation rate, based on images of the bubbles recorded during the irradiations. Temperature profiles resulting from the CFD calculations are compared to experimental measurements.

Solution vessel model

The geometry and liquid height used for both the MCNP and Fluent calculations are the same as described in the previous report.[2] The depth of the liquid (aligned with beam direction) is approximately 16 cm, and the width is approximately 20 cm. A cooling tube with an outer diameter of 3.81 cm runs through the center of the vessel. The steady-state volume-average temperature calculated from the thermocouple measurements was reported to be 45.2 ±0.1°C [3], and although no volume-average temperature was reported for the 15 kW case, the mean temperature calculated from the thermocouples was plotted, and it appears to be 50.5 ±0.1°C [3]. The initial fill volume was reported to be 20 L, so by using the decreased liquid density at the elevated temperatures, the liquid height at steady-state operation was calculated to be 63.70 and 63.86 cm for the 12 and 15 kW experiments, respectively. Figure 1 shows the SolidWorks model of the as-built stainless steel solution vessel and the thermocouple probe locations. Each thermocouple

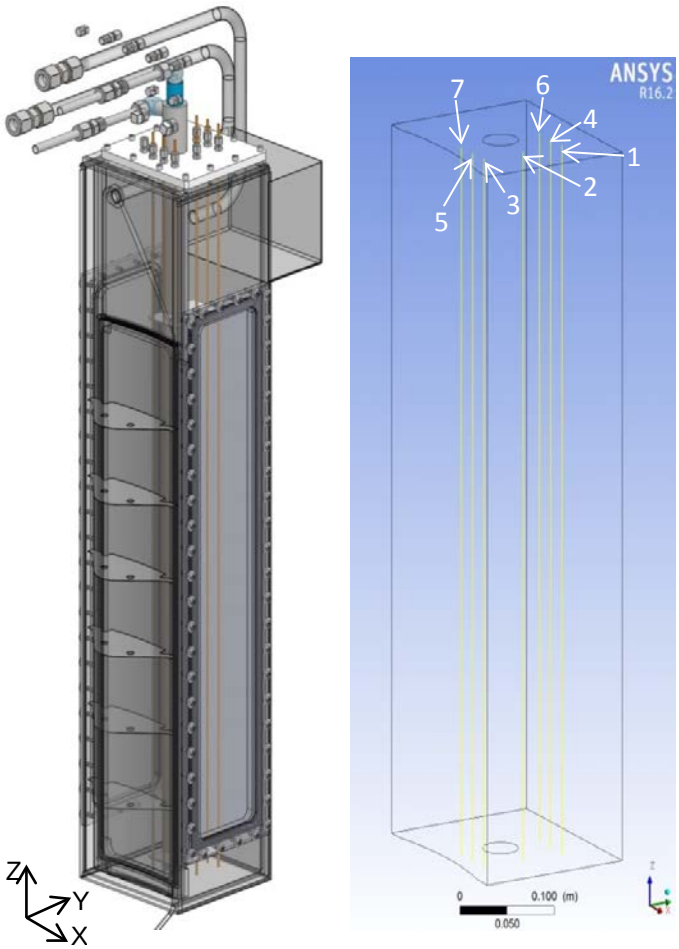

Figure 1. As-built vessel model and thermocouple locations.

[1] Buechler, Argonne Bubble Experiment Thermal Model Development, LA-UR-15-29280.
[2] Buechler, Argonne Bubble Experiment Thermal Model Development II, LA-UR-16-24607.
[3] Chemerisov et al., Experimental Results for Direct Electron Irradiation of a Uranyl Sulfate Solution: Bubble Formation and Thermal Hydraulics Studies, ANL/NE-15/19.

records temperatures at five vertical locations. Two cooling channels remove the heat during the experiment. A rectangular channel directs water down along the front face of the vessel, across the bottom, and up the back face. A nested tube also provides cooling by directing water down along the outer annular channel and back up through an inner tube.

Heat generation and model setup

The CFD model was set up the same way as described in the reports "Argonne Bubble Experiment Thermal Model Development.[1,2] The only changes made were to the 15 kW bubble diameter, the wall boundary conditions, and the gas generation rates. The volume integrals of the power profiles for the 12 and 15 kW cases were 6029 and 7512 W, respectively, as they were in the previous analysis[2]. The beam power was 12 and 15 kW for the two experiments, but only about half of the beam power was deposited in the solution. The power deposition profiles of the rastered electron beam are shown for the 12 kW and 15 kW cases in Figure 2. The units are W/m^3, and the electron beam is traveling in the Y-direction. The top surface of the liquid domain for the 15 kW case is 1.6 mm higher than for the 12 kW case. The data values displayed for the power deposition and the results profiles appearing later in the report are interpolated from mesh vertex values.

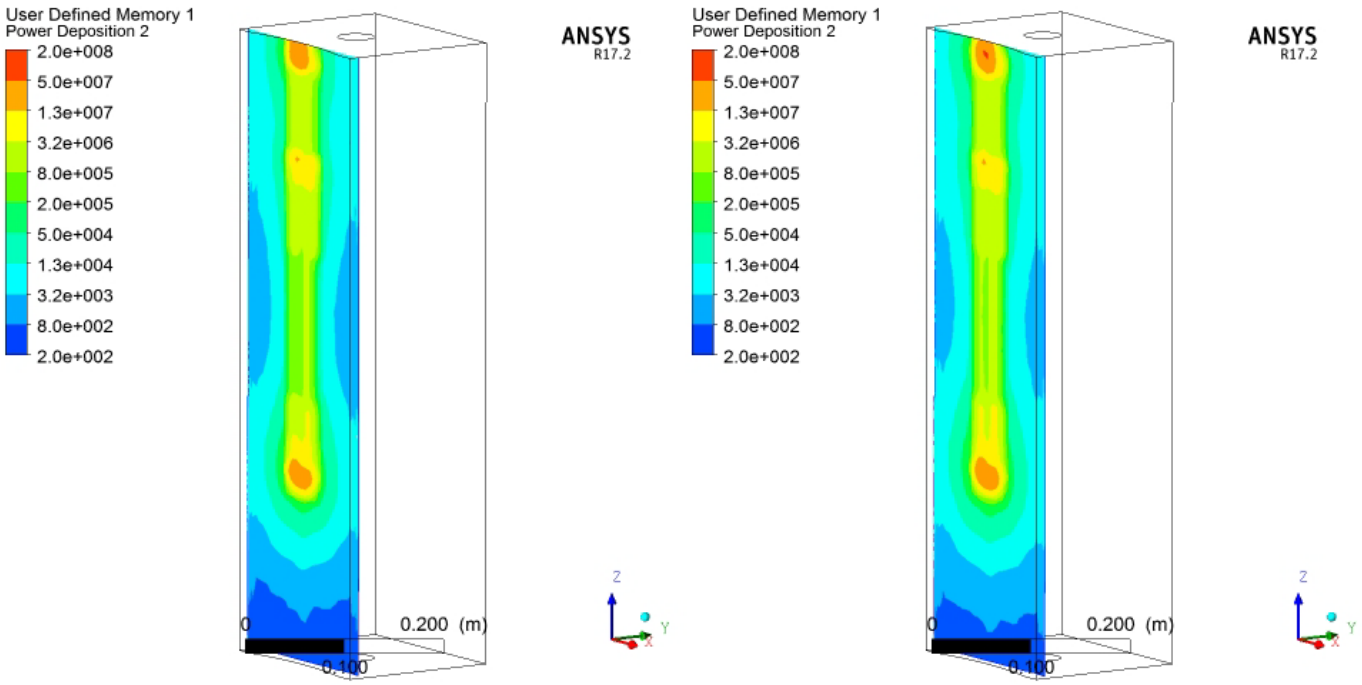

Figure 2. Power deposition profiles used as energy source definitions for 12 (left) and 15 kW (right) cases.

As in the previous study, temperature-dependent functions for thermal conductivity and viscosity were specified for uranyl sulfate at a concentration of 135 gU/liter, and a constant specific heat of 3627.97 J/kg-K was used. The Boussinesq buoyancy approximation was used to model the natural convection. Density values of 1142 and 1139 kg/m^3 were used for the uranyl sulfate material for the 12 and 15 kW cases, respectively. These values and those used for the thermal expansion coefficients correspond to temperatures that match the converged steady-state result for the volume-average liquid temperature to within 0.5°C. Thermal expansion coefficient values of 0.00047 and 0.00050 K^{-1} were used for the 12 and 15 kW cases, respectively.

The calculations were run in steady-state (pseudo-transient) mode, and time scale factors of 0.1 and 0.05 were used for the 12 and 15 kW cases, respectively. These time scale factors resulted in pseudo-timestep values of 16.6 and 8.3 ms. The smaller timescale factor used for the 15 kW case improved the energy and mass balances.

Calculations are considered converged when the integrated surface heat flux matches the total heat generation to within 0.5%. The mass balance is also checked to verify that the mass flow of the gas leaving the top surface matches the mass generation rate to within 3%. These quantities fluctuate during the calculation, so results for these values are averaged over 10,000 iterations. Calculations converge after approximately 130,000 iterations.

Bubble diameters of 205 and 267 µm were measured during 6 kW and 12 kW experiments, but no bubble diameter measurement was made at 15 kW.[3] In the previous study, a bubble diameter of 267 µm was specified for both the 12 and 15 kW cases. In the current study, 267 µm is still specified for the 12 kW cases, but a larger bubble diameter is specified for the 15 kW cases, accounting for the observation of increased bubble diameter with power density. The bubble diameters measured during the 6 and 12 kW cases were linearly extrapolated with the power level to determine a diameter of 298 µm for the 15 kW case.

Boundary conditions update

In the current study, the linearly-varying temperature boundary conditions were replaced with convection boundary conditions. The convection boundary condition allows the temperature to change based on the magnitude of the heat transfer across the wall.

The wall thickness, heat transfer coefficient (HTC), and free-stream temperature (FST) are required to define a convection boundary condition on a wall. Table 1 shows the values used for each wall in the 12 and 15 kW calculations. A thermal conductivity of 16 W/m^{2}K was specified for the stainless steel wall material. The total flow through the channels is 50 gpm. The flow through each channel was calculated by dividing the total flow according to the flow area of the channel. Based on these flow rates and the fractional power removed by each cooling channel, which was determined in previous Fluent simulations, the temperature increase was calculated for the front face of the rectangular channel, the back face of the rectangular channel, and the cooling tube. The midpoint temperature for each of these three cooling channel sections was used as the FST. The average of the FST values for the front and back channels was used for the bottom channel, which removes almost no heat. The heat transfer coefficients were determined using the Dittus-Boelter correlation for turbulent flow through circular tubes.[4] Because the flow is turbulent, the correlation for circular tubes is also valid for rectangular channels.

Table 1. Wall boundary condition parameters specified for 12 and 15 kW cases.

	SS wall thickness (cm)	12 kW		15 kW	
		HTC (W/m^{2}K)	FST (C)	HTC (W/m^{2}K)	FST (C)
Cooling Tube	0.089	7303	20.14	7303	20.26
Front Rectangular Channel	0.122	8660	19.88	8660	19.93
Back Rectangular Channel	0.305	7256	20.19	7256	20.33
Bottom Channel	0.305	7256	20.03	7256	20.13

A 12 kW calculation with convection boundary conditions was performed using the same conditions, including mass generation rate, as the 12 kW calculation performed previously using the linearly-varying temperature profile[2]. Wall temperature results for the two calculations are compared in Figure 3. The converged volume-average liquid temperature results differ by just 1°C for the two calculations, but the wall temperatures differ by as much as 13°C.

[4] Incropera, Fundamentals of Heat and Mass Transfer, 4th Ed., Wiley, p. 445.

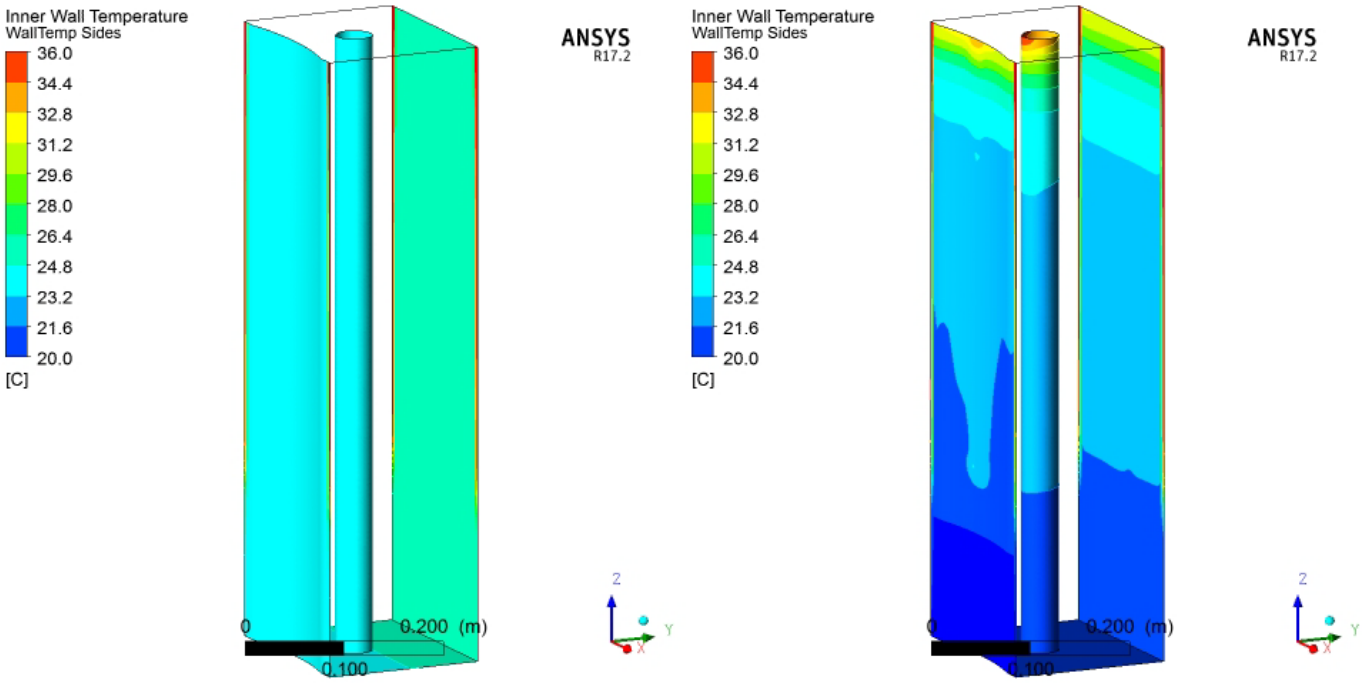

Figure 3. Cold wall temperature results using linearly-varying temperature (left) and convection (right) boundary conditions.

Gas generation rate update

In the previous study, the gas generation rates were estimated based on concentration measurements collected with a gas chromatograph during the irradiation. The rate of radiolytic gas production was not allowed to reach steady-state during the experiments, and the delay between the gas generation and the measurement at the gas chromatograph was significant, due to the large mixing volume of the gas system. In the current study, gas generation rates were selected to match images recorded during the irradiation experiments. The results of the calculations using these selected rates are compared to results from calculations using the gas generation rates determined from the gas chromatograph measurements.

Images were taken from the videos posted on YouTube of the 12 kW[5] and 15 kW[6] tests[3]. An image half way through each video time period was selected for analysis. The bubble dynamics appeared constant throughout the videos, which were each about a minute long, so these images are believed to be fair representations of the solution vessel dynamics for each test. A 1 cm^2 area near the top of each image was analyzed to determine the bubble volume fraction. In the same manner as described in the ANL report[3], the thermocouple diameter (1/8”) was used to determine the scale of the images shown in Figure 4 and Figure 5. A square with sides equal to approximately three times the width of the thermocouple, or 0.95 cm, was overlaid on the image. The depth of field of the focal plane is reported to be rather small[3], so it is estimated that the bubbles that can be seen in the square are spread out over a depth of 1 cm. The bubbles present inside the square are, therefore, assumed to exist within a 1 cm^3 volume.

An average bubble diameter of 267 µm was measured during the 12 kW experiment[2], and it is estimated that 100-300 bubbles can be seen in the square. By calculating the volume of a single 267 µm bubble, multiplying by the number of bubbles counted and dividing by the volume of 1 cm^3, the bubble volume fraction is calculated to be 1.0e-3 to 3.0e-3 in this top-center region.

[5] https://www.youtube.com/watch?v=meNm3ZFs0wY
[6] https://www.youtube.com/watch?v=5TjWLTmBo6s

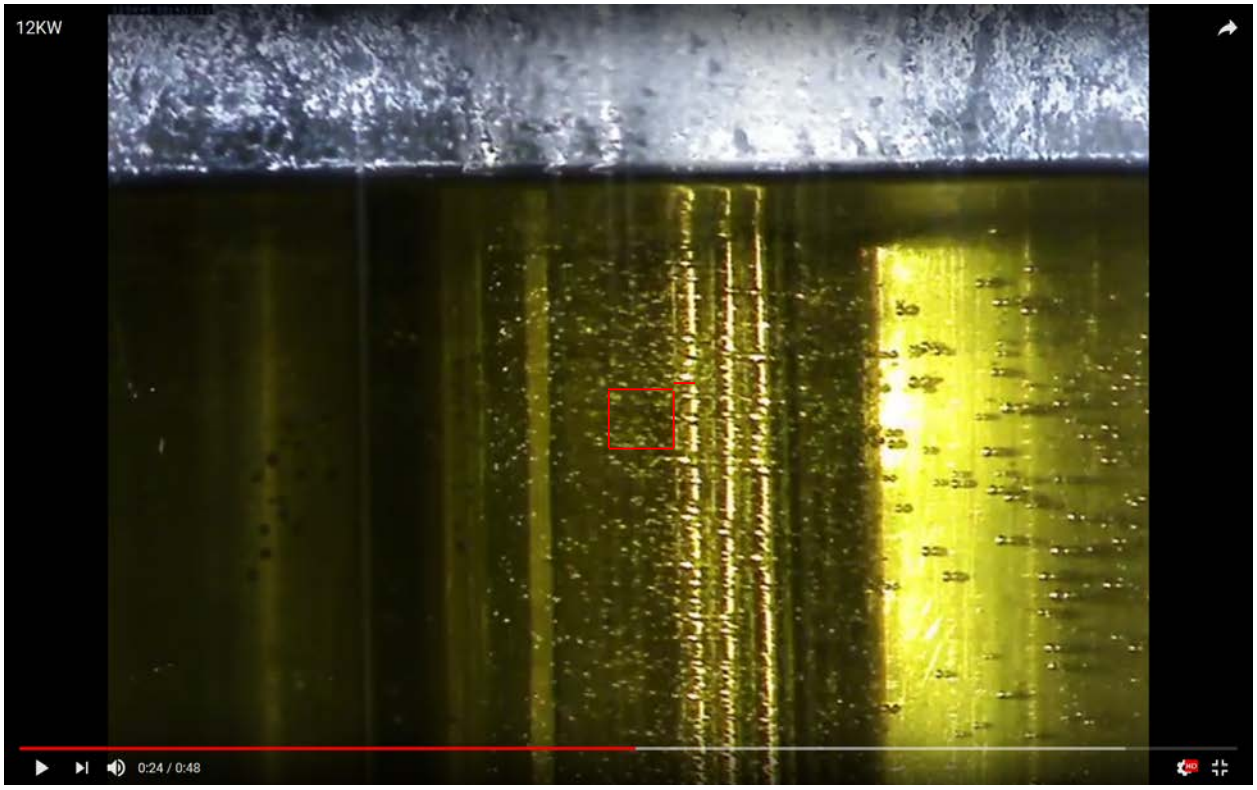

Figure 4. Image from video of 12 kW irradiation at ANL

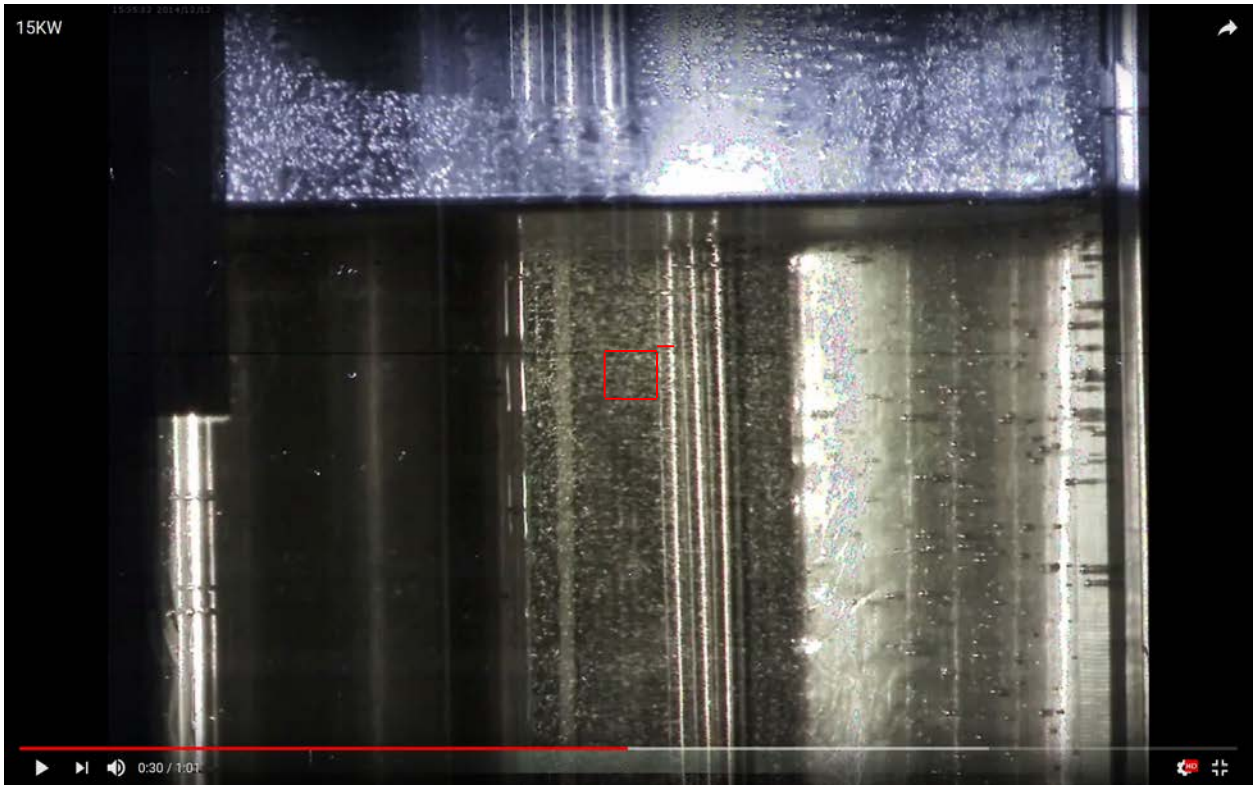

Figure 5. Image from video of 15 kW irradiation at ANL

Gas generation rates of 1.4e-11, 3.0e-11, and 4.4e-11 kg/s/W were used as trial values in the simulations and were found to produce volume fraction values in the top-center region between 1.6e-3 and 2.7e-3. The bubble volume fraction values at the top of the vessel are not steady throughout the calculation but oscillate around an average value by as much as 60%. To determine the average value, 20 sets of bubble volume fraction results at the top of thermocouple 7 (x=0.0, y=5.86, z=61.54 cm) were recorded at intervals of 2,000 iterations. The average volume fraction at the top center of the vessel was determined by averaging these 20 values.

Looking at the same region of the vessel for the 15 kW experiment in Figure 5, it is estimated that 200-400 bubbles are in the square. By calculating the volume of a single 298 µm bubble, multiplying by the number of bubbles counted and dividing by 1 cm^3, the bubble volume fraction is calculated to be 2.8e-3 to 5.5e-3 in this top-center region. The same gas generation rates as were used in the 12 kW simulations were used in the 15 kW simulations, 1.4e-11, 3.0e-11, and 4.4e-11 kg/s/W. These rates were found to produce volume fraction values in the top-center region between 2.0e-3 and 3.3e-3.

The simulation results for the total mass generation (kg/s) for the 12 kW case using these trial gas generation rates (kg/s/W) are between 8.4e-8 and 2.7e-7 kg/s. The results for the 15 kW case are between 1.0e-7 and 3.3e-7 kg/s. These mass generation values are almost three orders of magnitude higher than the rates calculated from the gas chromatograph measurements. The mass generation values calculated from the gas chromatograph measurements were 2.87e-10 and 6.1e-10 kg/s for the 12 and 15 kW cases, respectively. Calculations were also performed for these lower mass generation values by specifying mass generation rates of 4.7e-14 kg/s/W and 8.2e-14 kg/s/W for the 12 and 15 kW cases, respectively. These calculations produced mass generation values matching the gas chromatograph measurements, and the top-center volume fraction results were 7.1e-6 and 1.4e-5 for the 12 and 15 kW cases, respectively. These volume fractions correspond to bubble counts of just 0.7 and 1.0 bubbles per cubic centimeter. Although the volume fractions determined from the images are very rough estimates, these calculations indicate that more bubble generation took place than was detected by the gas chromatograph in the experiment. The volume-average volume fraction and top-center volume fraction results for the three selected gas generation rates are plotted along with the volume fraction results for the mass generation rates determined from the gas chromatograph measurements in Figure 6.

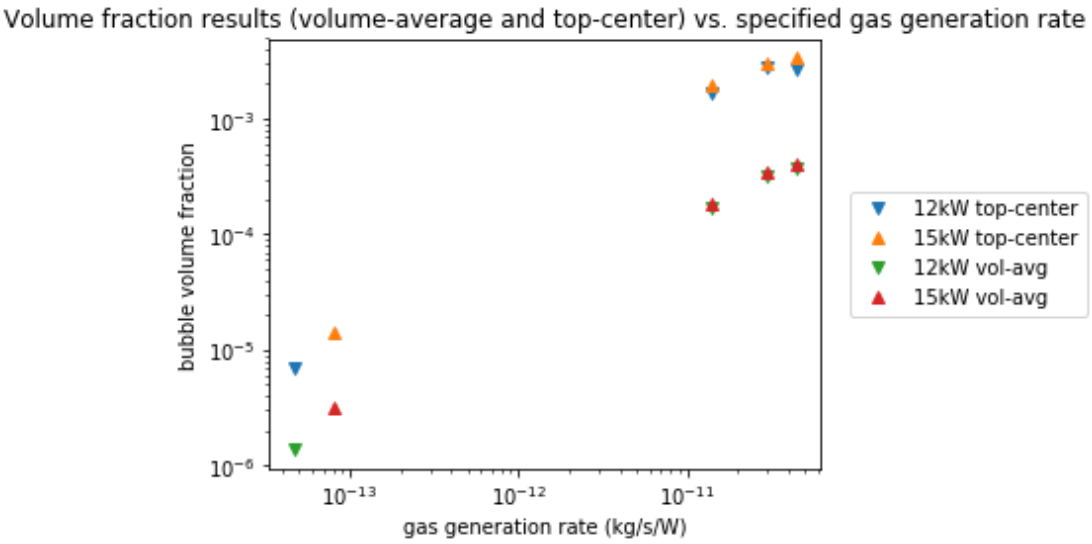

Figure 6. Average bubble volume fraction values for 12 and 15 kW cases and three gas generation rates.

Temperature results from the calculation using a gas generation rate of 4.7e-14 kg/s/W matched a calculation performed with no gas generation at all.[2] Heat transfer enhancement seems to be insignificant until bubbles are generated at a certain rate. This study aims to determine what that rate is for this system and if it is reasonable to believe that this rate could have been generated in these experiments, based on recorded images.

Calculation results

The steady-state calculation results for the 12 and 15 kW beam cases are presented in Table 2.

Table 2. Fluent calculation results for 12 and 15 kW.

Beam power (kW)	Bubble diameter (μm)	Gas generation rate (kg/s/W)	Max Fuel Temp (°C)	VolAve Fuel Temp (°C)	Min Z-Veloc Fuel (cm/s)	Max Z-Veloc Fuel (cm/s)	Max Vertical Veloc Bubbles (cm/s)	VolAvg Vertical Veloc Bubbles (cm/s)	Vol Frac Bubbles at top, center	VolAvg Vol Frac Bubbles
12	267	4.72e-14	123.3	51.6	-4.8	5.2	8.3	2.85	7.1e-6	1.4e-6
		1.4e-11	112.9	52.4	-6.3	5.7	8.8	2.94	1.6e-3	1.7e-4
		3.0e-11	88.5	53.3	-5.7	6.8	10.0	2.96	2.7e-3	3.2e-4
		4.4e-11	75.6	52.5	-7.6	11.0	14.2	2.94	2.7e-3	3.8e-4
15	298	8.17e-14	133.1	56.8	-5.7	6.0	9.8	3.49	1.4e-5	3.1e-6
		1.4e-11	123.6	57.6	-6.7	5.4	9.1	3.52	2.0e-3	1.9e-4
		3.0e-11	100.1	58.4	-6.3	7.6	11.5	3.56	3.1e-3	3.5e-4
		4.4e-11	84.3	57.6	-9.1	9.1	13.0	3.53	3.3e-3	4.1e-4

The temperature results at the top of the tank are above boiling for both cases at the low gas generation rates. If the average of the values for volume-average temperature for the three trial mass generation rates is taken for each beam power level, volume-average temperatures of 52.7 and 57.9 are calculated for the 12 kW and 15 kW cases, respectively. For both power levels, the difference between the volume-average temperature result from the simulation and the temperature calculated from experimental measurements is about 7.5°C.

Temperature results are shown for profiles aligned with each of the seven thermocouple probes for the 12 and 15 kW cases in Figure 7 and Figure 8. The temperature profiles are also not steady throughout the calculation, so 20 sets of temperature results were recorded at intervals of 2,000 iterations. The average temperature profile for each thermocouple probe was determined by averaging these 20 values. The measurements recorded by the thermocouple probes are also shown on the plots.

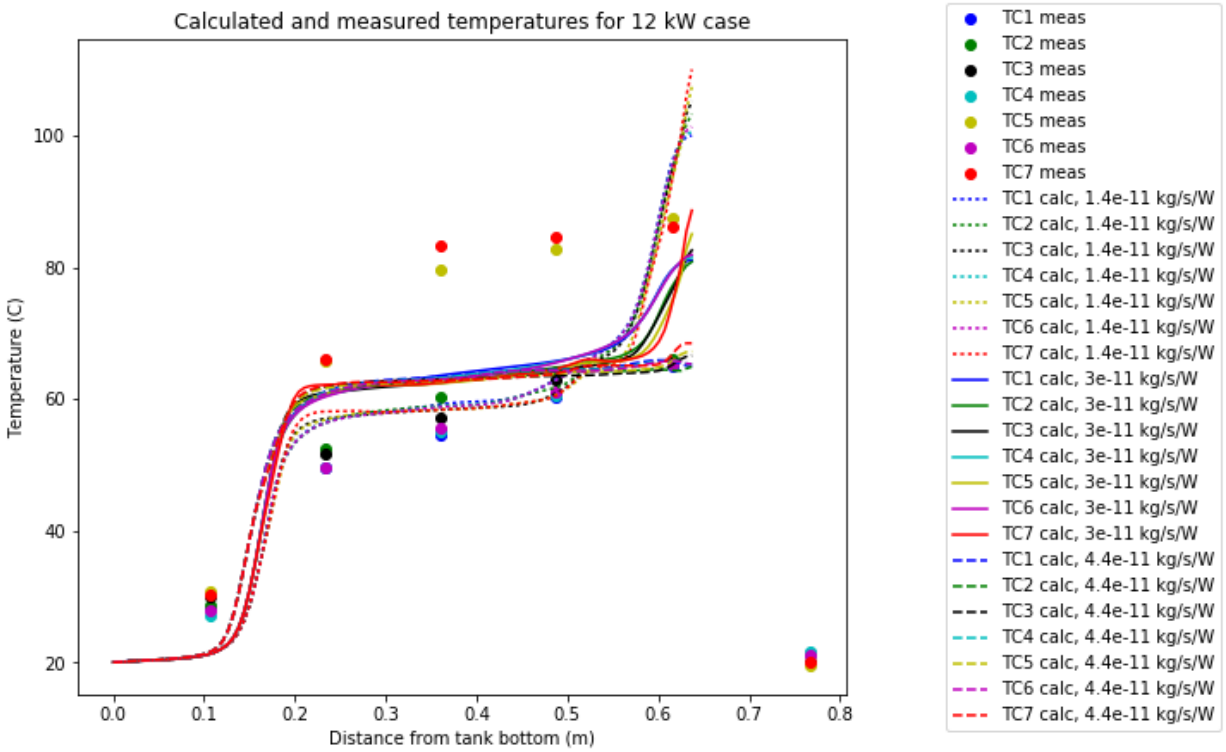

Figure 7. 12 kW case: Temperature measurements (circles) compared to temperature profiles from simulation results (solid lines).

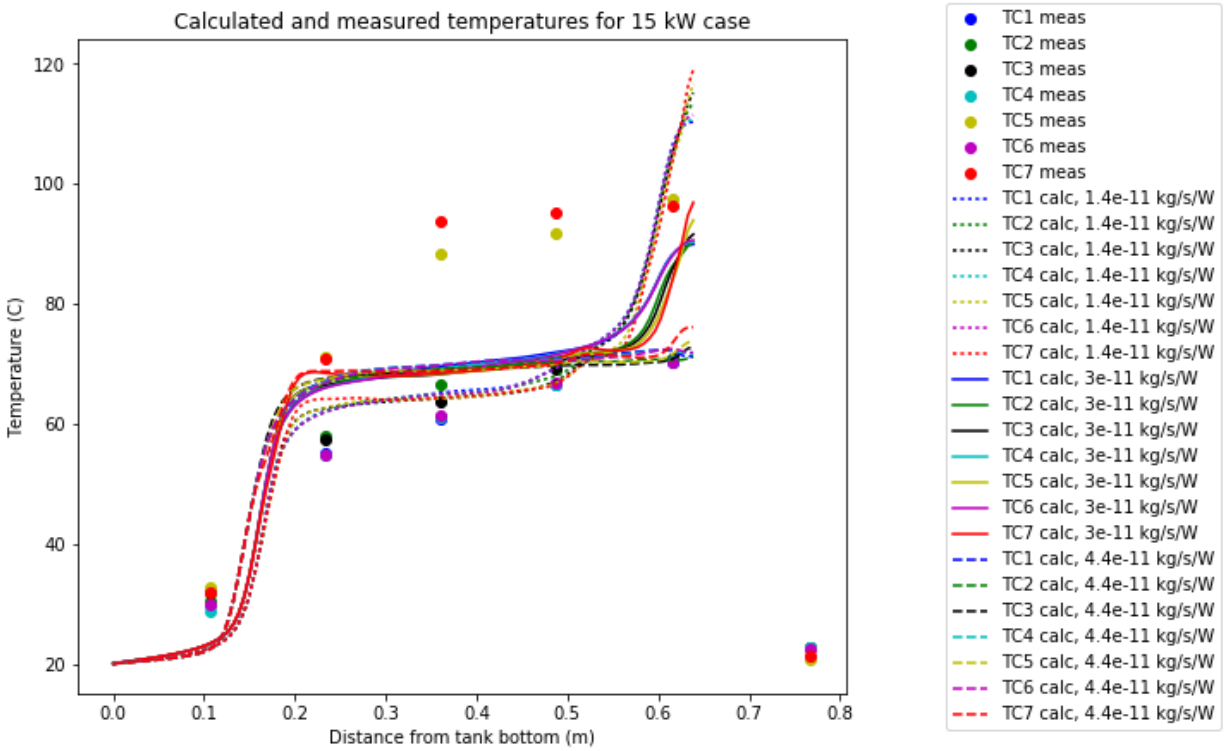

Figure 8. 15 kW case: Temperature measurements (circles) compared to temperature profiles from simulation results (solid lines).

The 12 and 15 kW cases exhibit similar temperature trends. The top location for each of the seven probes was above the liquid level, so those measurements are near room temperature. TCs 5 and 7 were directly heated by the beam during the experiment, so their readings are not to be considered valid measurements of the liquid

temperature but are shown along with the other measurements. The calculated temperatures were also highest at the top of the tank for these two thermocouples for all three gas generation rates. For both the measurements and calculations, temperature variations between horizontal positions are small compared to variations from top to bottom. To simplify the plots, average values for the calculated and measured temperature are shown in Figure 9 and Figure 10. The calculated and measured temperature for TCs 5 and 7 are not included in the averages, and the temperatures measured at the top of the tank are not shown. Results are also included from the calculations performed with gas generation rates corresponding to the measured gas generation for the 12 and 15 kW cases.

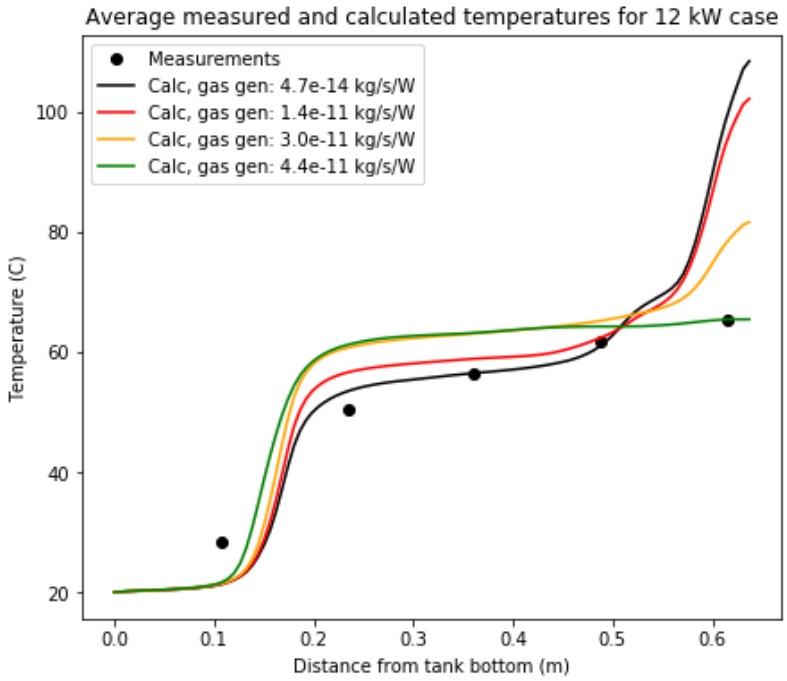

Figure 9. 12 kW case: Average measurements (circles) compared to average simulation results (solid lines).

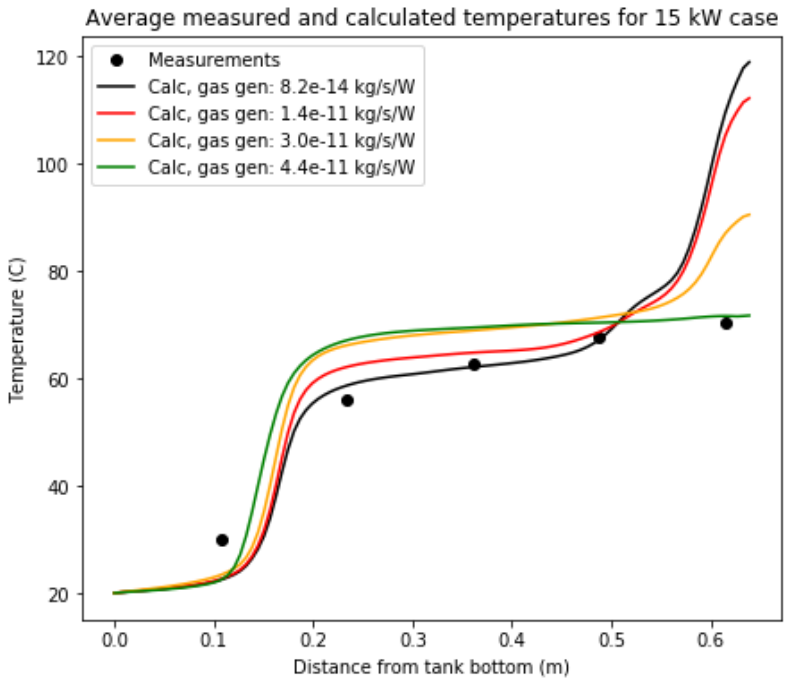

Figure 10. 15 kW case: Average measurements (circles) compared to average simulation results (solid lines).

Calculated temperatures using the low estimate for gas generation rate match measured temperatures in the lower portion of the tank better than temperatures calculated using the high estimate. At the top of the tank, the opposite is true: calculated temperatures using the high estimate for gas generation rate match measured temperatures better than temperatures calculated using the low estimate. Temperature results for calculations using a gas generation rate of zero would match the results presented for the 4.7e-14 kg/s/W rate. Calculations using a gas generation rate larger than 4.4e-11 kg/s/W would produce flat temperature profiles, similar to the 4.4e-11 kg/s/W calculations, at even lower temperatures, as shown in the gas generation sensitivity analysis performed in the previous study.[2]

These results are consistent with other analyses indicating that bubble generation helps to enhance heat transfer and produces a more homogenous vertical temperature profile.[7, 8] These calculations show that the gas generation rate at which this enhancement occurs is between 1.4 and 4.4e-11 kg/s/W. This transition is similar to the heat transfer enhancement transition that was noticed in the SUPO experiments. The gas generation in the SUPO experiments was 2.78e-9 kg/s/W.[9, 10] This is much higher than in the current experiment, because neutrons are much more likely to interact with water and produce radiolytic gas than electrons. Still, at low SUPO power levels, a transition point was found below which the heat transfer characteristics are indistinguishable from a single phase system, and above which the heat transfer is significantly enhanced by radiolytic gas bubbles.[11]

For the SUPO experiment, the gas generation density at which the heat transfer enhancement occurs is around 2 g/s/m^3. For the current study of the Argonne Bubble Experiment, the transition value for gas generation density was found to be around 1 g/s/m^3. The gas generation density is plotted (for the 1.4e-11 and 4.4e-11 kg/s/W mass generation rates) in Figure 11. The units in the legends are kg/s/m^3.

[7] Durham, Radiolytic-Gas Bubbling Improves Convective Heat Transfer in Supo, Nucleonics, 1955.
[8] Buechler, Aqueous Solution Vessel Thermal Model Development, LA-UR-15-23537.
[9] Bunker, Status Report on the Water Boiler Reactor, LA-2854, 1963.
[10] King, Design and Description of Water Boiler Reactor, Proceedings of the International Conference on the Peaceful Uses of Atomic Energy, 1955.
[11] Wass, Supo Thermal Model Development II, LA-UR-17-25822.

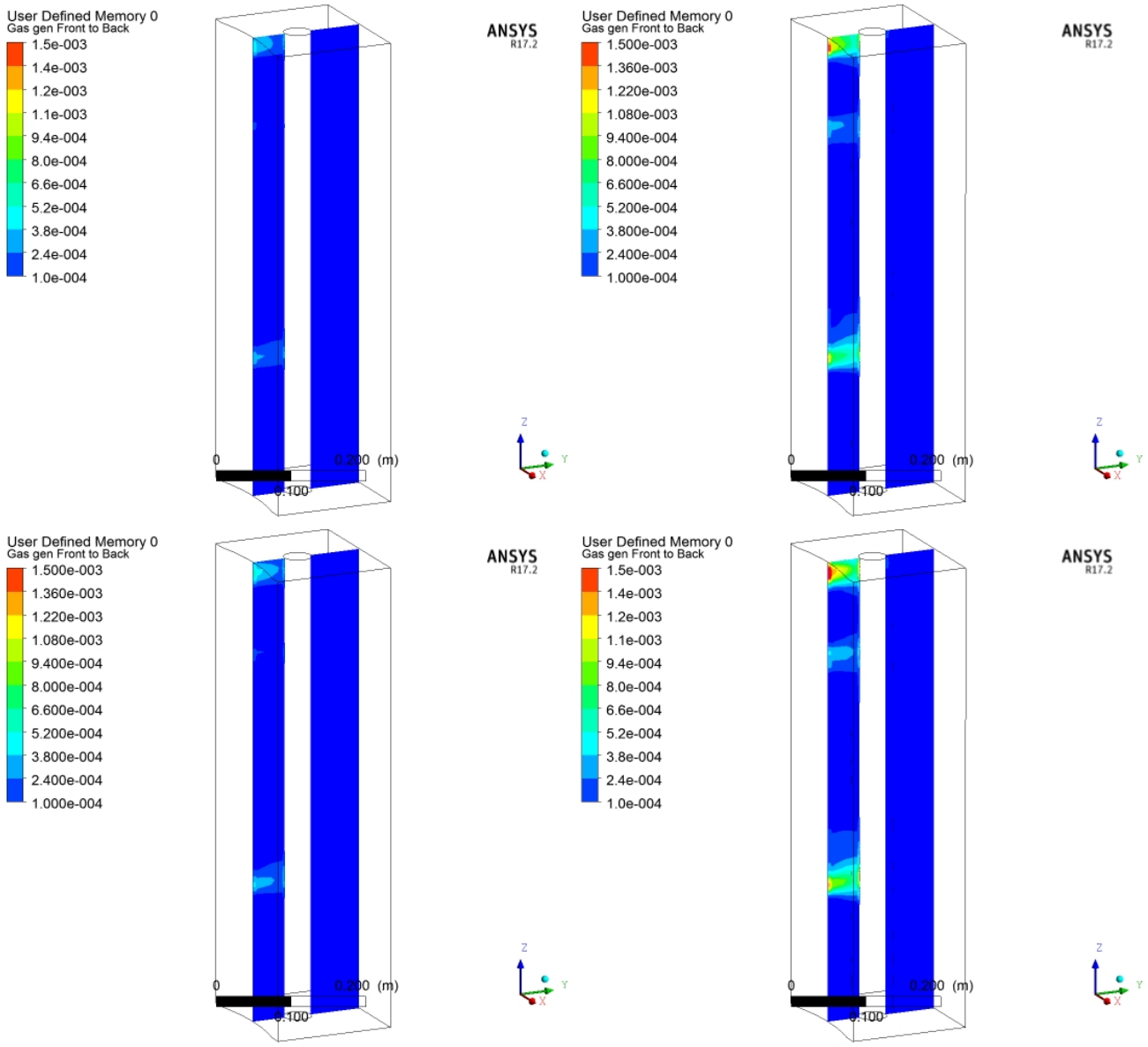

Figure 11. Steady-state gas generation density for 12 kW (top) and 15 kW (bottom) cases. Images on left are for 1.4 kg/s/W, and images on right are for 4.4 kg/s/W.

Temperature results are shown for the 12 and 15 kW cases in Figure 12, (for the lowest and highest mass generation rates), and bubble volume fraction results are shown in Figure 13.

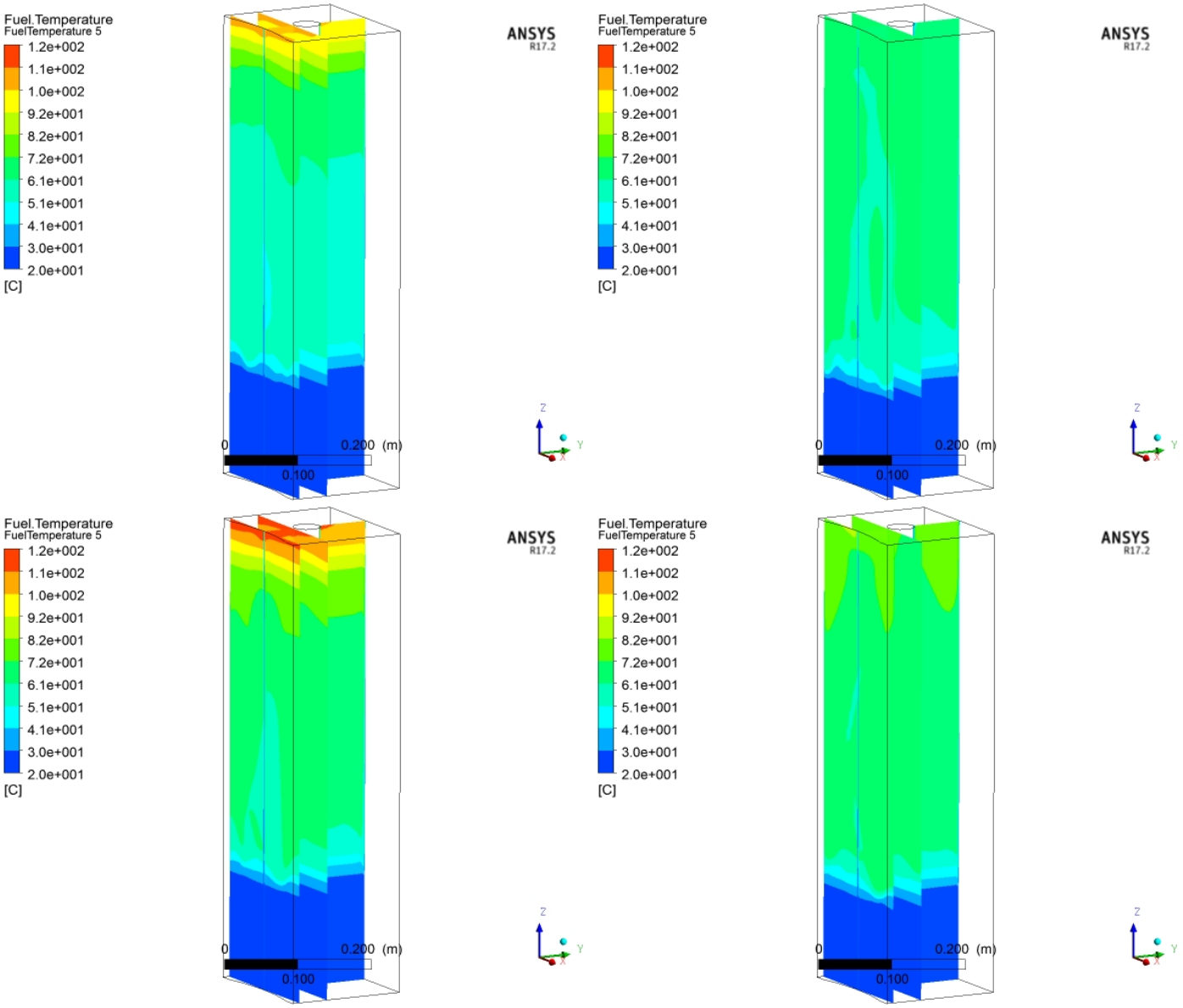

Figure 12 Steady-state liquid temperature for 12 kW (top) and 15 kW (bottom) cases. Images on left are for 1.4 kg/s/W, and images on right are for 4.4 kg/s/W.

The simulation results for the bubble volume fraction profiles qualitatively match the reported experimental observations.[3] It was reported that a volume fraction estimate was not feasible from the bubble size and distribution measurements. The solution level height increase would not have been detected at these gas generation rates given that the uncertainty in the measurement of the solution height change was reported to be ± 0.20 mm.[3]

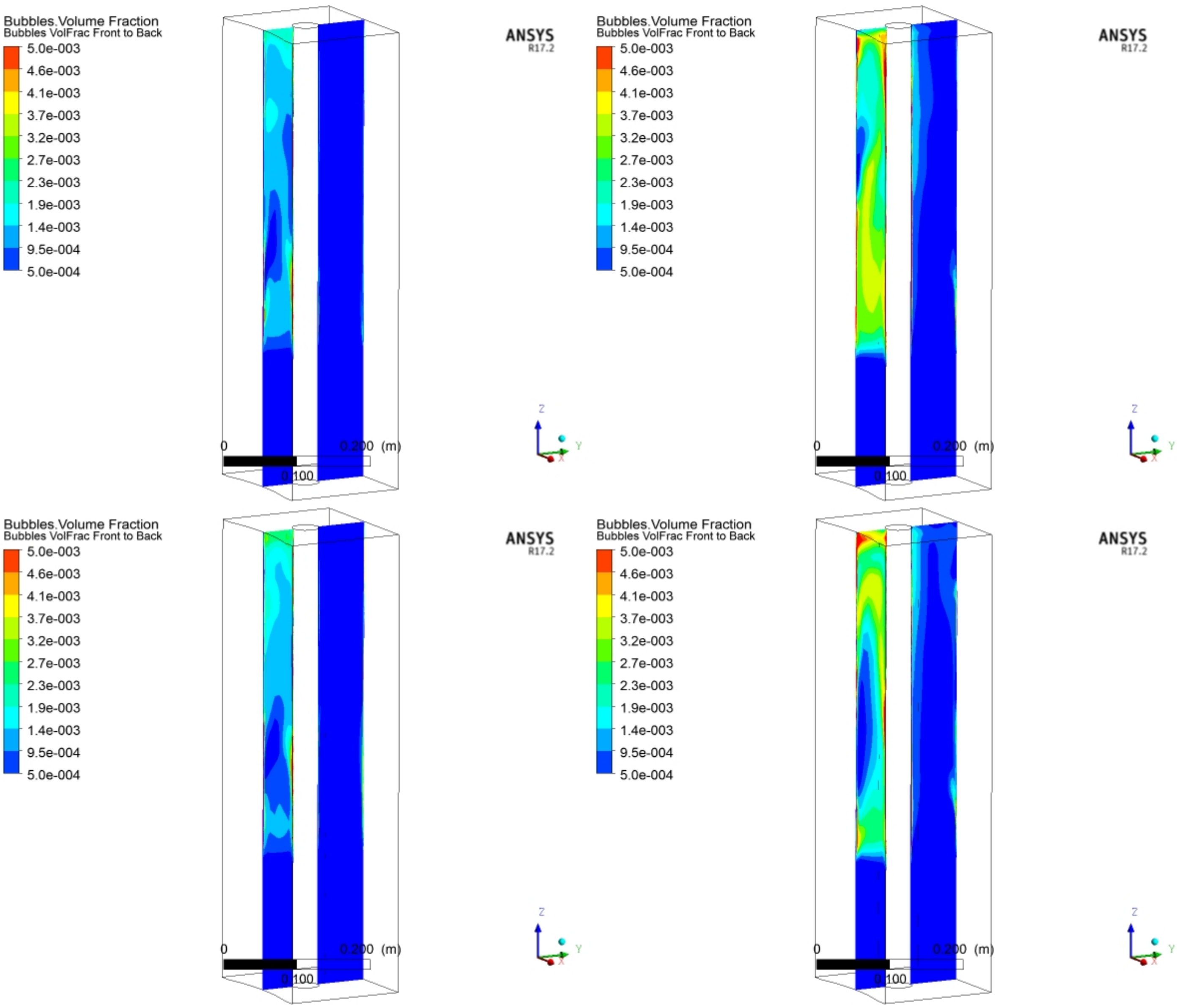

Figure 13. Steady-state volume fraction profiles for 12 kW (top) and 15 kW (bottom) cases. Images on left are for 1.4 kg/s/W, and images on right are for 4.4 kg/s/W.

The liquid vertical velocity profiles are shown in Figure 14. The fuel velocity directions and magnitudes for the for the lowest gas generation rate roughly match those observed in the 12 kW experiment: 1-2 cm/s near the front and top of the tank, and approximately -3 cm/s at the rear of the central tube near the mid-height.[3] The fuel velocities for the highest gas generation rate are about twice those reported for the 12 kW experiment. No bubble velocity measurements were reported for the 15 kW case.

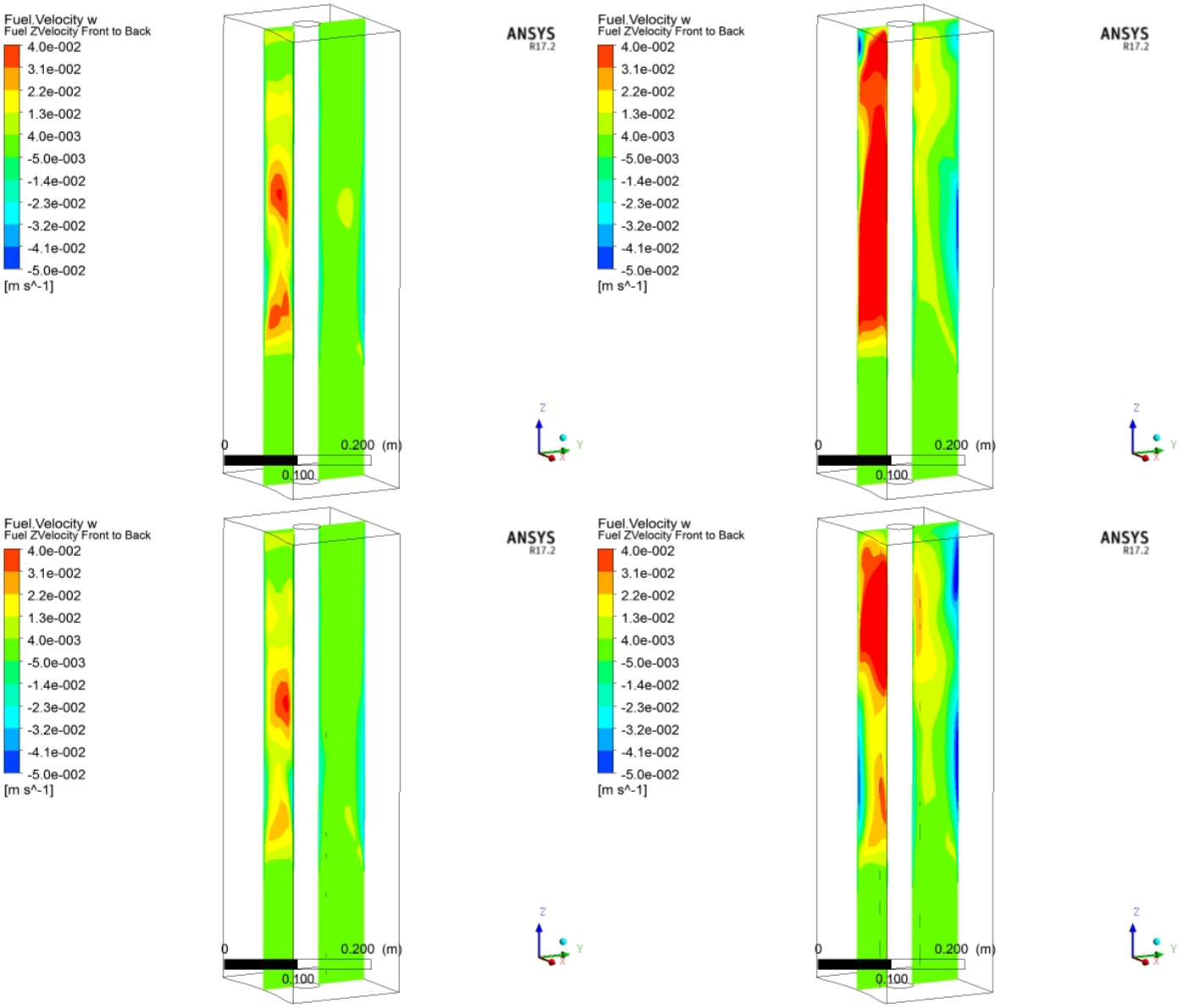

Figure 14. Steady-state vertical fuel velocity for 12 kW (top) and 15 kW (bottom) cases. Images on left are for 1.4 kg/s/W, and images on right are for 4.4 kg/s/W.

The bubble vertical velocity profiles are shown in Figure 15. The calculated vertical bubble velocity near the top of the tank was 4-5 cm/s for the lowest gas generation rate, matching the measured vertical bubble velocity in that region for the 12 kW case.[3] No bubble velocity measurement was reported for the 15 kW case.

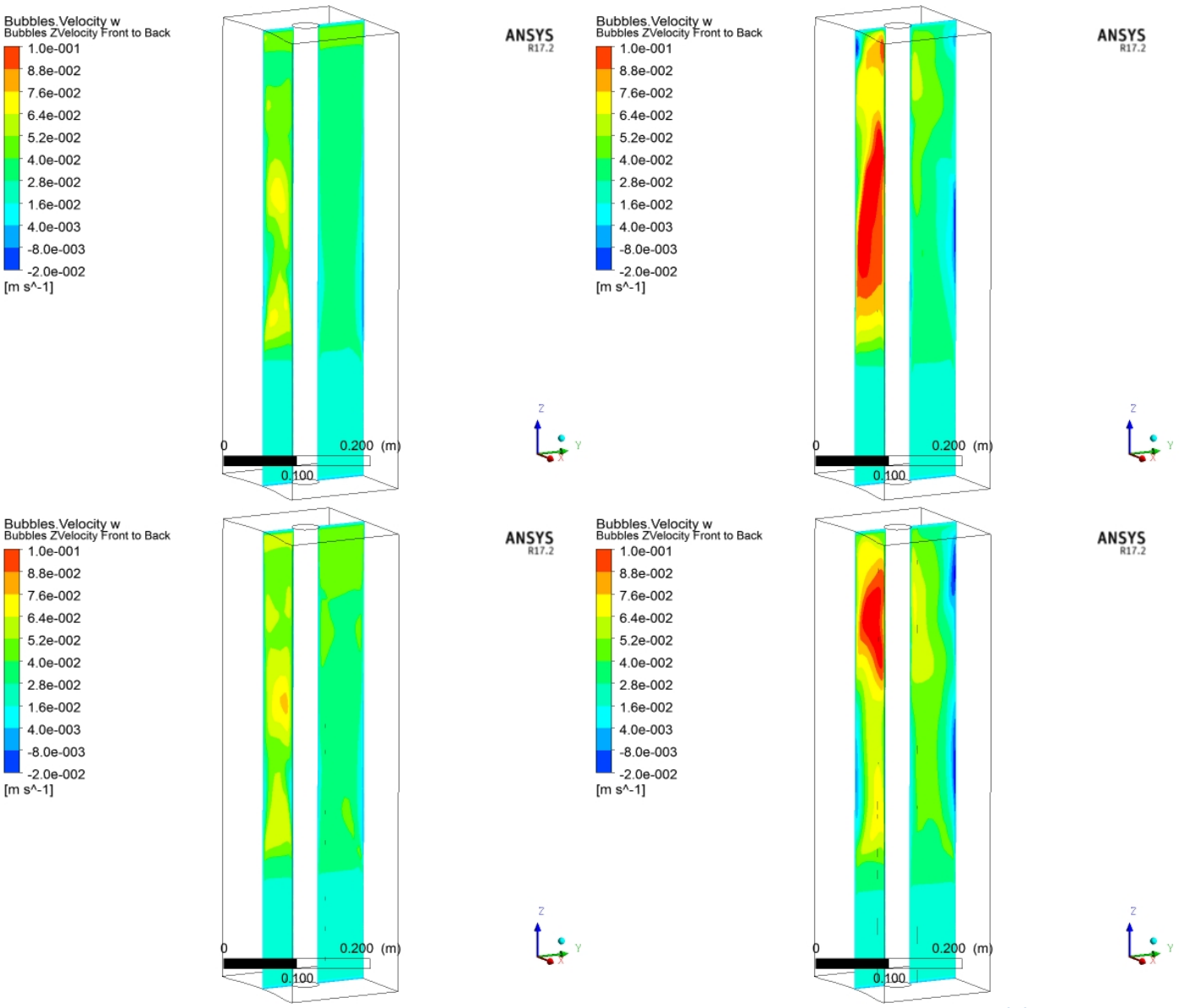

Figure 15. Steady-state bubble vertical velocity for 12 kW (top) and 15 kW (bottom) cases. Images on left are for 1.4 kg/s/W, and images on right are for 4.4 kg/s/W.

Conclusion

A threshold gas generation rate must be achieved in order to generate the heat transfer enhancement that radiolytic gas bubbles have been known to produce in aqueous reactor solution vessels. By specifying a gas generation rate on the order of 1e-11 kg/s/W, results for bubble volume fraction at the top of the tank were produced which are consistent with the bubble fractions estimated from the images recorded during the experiments. The calculations performed using gas generation rates between 1.4e-11 and 4.4e-11 kg/s/W produced temperature profile results that were in reasonable agreement with measured profiles. The calculations using the low gas generation rates matched the measured profiles better in the lower portion of the tank, and the calculations using high gas generation rates matched the measured profiles better in the top portion of the tank. Based on the bubble images, it is reasonable to believe that the bubble generation rate during these experiments was high enough to provide heat transfer enhancement at the top of the vessel. Accurate gas generation rate measurements in future experiments could provide key input data for these multi-phase CFD calculations.